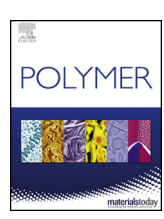


Contents lists available at ScienceDirect

Polymer

journal homepage: www.elsevier.com/locate/polymer



Thermally cross-linked diaminophenylindane (DAPI) containing polyimides for membrane based gas separations



Michelle E. Dose^a, Malgorzata Chwatko^b, Ivo Hubacek^c, Nathaniel A. Lynd^b, Donald R. Paul^a, Benny D. Freeman^{a,*}

- ^a McKetta Department of Chemical Engineering, Center for Energy and Environmental Resources, Texas Materials Institute, The University of Texas at Austin, 10100 Burnet Road Building 133 (CEER). Austin. TX. 78758. United States
- b McKetta Department of Chemical Engineering, The University of Texas at Austin, 200 E Dean Keeton St., Austin, TX, 78712, United States
- ^c Dottikon Exclusive Synthesis AG, P.O. Box, 5605, Dottikon, Switzerland

HIGHLIGHTS

- A polyimide containing 6FDA, DAPI, and DABA, 6FDA-DAPI/DABA, was synthesized and characterized.
- 6FDA-DAPI/DABA was cross-linked above its T_g by thermal decarboxylation.
- Cross-linking increased d-spacing, and permeability increased by 30%.
- C₂H₄/C₂H₆ and CO₂/CH₄ ideal selectivities increased with cross-linking.

ARTICLE INFO

Keywords: Diaminophenylindane (DAPI) Polyimides Thermal decarboxylation Cross-linking Pure gas permeability

ABSTRACT

This study aims to expand structure-property relationships of diaminophenylindane (DAPI)-containing polyimides and the influence of thermal cross-linking on gas transport properties of such materials. A polyimide synthesized from hexafluoroisopropylidene diphthalic anhydride (6FDA), DAPI, and diaminobenzoic acid (DABA) in a molar ratio of 0.5/0.33/0.17, 6FDA $_{0.5}$ -DAPI $_{0.33}$ /DABA $_{0.17}$, was crosslinked by thermal decarboxylation. After cross-linking, pure gas permeability of 6FDA $_{0.5}$ -DAPI $_{0.33}$ /DABA $_{0.17}$ increased with increased crosslinking time; gas permeability increased by about 30% after cross-linking at 353 °C for 40 min. This increase in permeability correlated with an increase in d-spacing measured by wide angle x-ray scattering, suggesting an increase in inter-chain spacing upon cross-linking. Minimal changes in O_2/N_2 and N_2/CH_4 selectivities occurred with increased thermal cross-linking time for 6FDA $_{0.5}$ -DAPI $_{0.33}$ /DABA $_{0.17}$. However, CO_2/CH_4 and C_2H_4/C_2H_6 pure gas selectivities increased with thermal treatment, suggesting a potential narrowing of free volume distribution.

1. Introduction and background

Polyimides are widely used and studied as gas separation membrane materials [1,2]. Those most commonly explored are solution processable, amorphous glassy polymers with rigid polymer backbones [3]. Polyimides are typically synthesized from at least one dianhydride and at least one diamine. Matrimid*, a commercially available polyimide, is comprised of two monomer units, 3,3',4,4'-benzophenone tetracarboxylic dianhydride (BTDA) and isomeric 5(6)-amino-1-(4-aminophenyl)-1,3,3-trimethylindane (diaminophyenylindane, DAPI). Its favorable transport properties have been attributed in part to the rigid, bulky, and isomeric structure of DAPI [4,5]. However, DAPI has not

been thoroughly investigated in other polymer structures due to its previously limited commercial availability. Previous studies incorporated DAPI with several dianhydrides, but those studies focused primarily on O_2/N_2 separations [4,5]. This work extends structure-property studies involving DAPI by incorporating the isomeric diamine into a thermally cross-linkable polymer. Cross-linking polyimides is reported to help reduce plasticization effects in applications such as natural gas and hydrocarbon separations [6,7].

Recently, there has been increasing interest in small scale hydrocarbon separations due to rapid growth of shale gas in the United States [8,9]. Currently, light hydrocarbons like ethane, ethylene, propane, and propylene are separated using fractional distillation [1,10]. High

^{*} Corresponding author. 10100 Burnet Rd., Bldg 133, Austin, TX, 78758, USA. E-mail address: freeman@che.utexas.edu (B.D. Freeman).

pressures and sub-ambient temperatures are needed to achieve these separations due to the small size and volatility differences between ethylene/ethane and propane/propylene (cf., Table S1) [11,12]. These features make olefin/paraffin separations among the most energy intensive processes in the petrochemical industry [1,10,13].

Previous studies have shown CO2 plasticization resistance can be improved by cross-linking carboxylic acid containing polyimides and polymers of intrinsic microporosity (PIM) by thermal decarboxylation [14-17]. Motivated by these prior results, this study focuses on crosslinking 6FDA_{0.5}-DAPI_{0.33}/DABA_{0.17}, which contains a molar ratio of 0.5/0.33/0.17 of 6FDA/DAPI/DABA, via thermal decarboxylation. The -C(CF₃)₂- linkages in 6FDA often increase polymer fractional free volume, thereby improving permeability while maintaining reasonable selectivity for a given gas pair [18-20]. Additionally, there is speculation in the literature that fluorocarbon functionality of -CF3 moieties may reduce solubility of hydrocarbons due to thermodynamically unfavorable interactions with hydrocarbons [20-22]. The inclusion of isomeric DAPI may also improve backbone rigidity and free volume due to its asymmetric, bulky structure [4]. Moreover, DABA provides reactive acid sites for cross-linking and/or modification [5,14–17,23,24]. A 2:1 ratio of DAPI:DABA was selected to permit this work to be compared with results from thermal cross-linking of 6FDA_{0.5}-DAM_{0.33}/ DABA_{0.17}, where DAM is 2,3-diaminomesitylene. 6FDA_{0.5}-DAM_{0.33}/ DABA_{0.17} was cross-linked at 389 °C, 15 °C above its glass transition temperature, for 40 min and showed improved plasticization resistance to CO_2 at high pressure [15].

Here, the synthesis and characterization of thermally cross-linked $6\mathrm{FDA}_{0.5}\text{-}\mathrm{DAPI}_{0.33}/\mathrm{DABA}_{0.17}$ is investigated. Pure gas permeability coefficients of $\mathrm{H_2}$, $\mathrm{O_2}$, $\mathrm{N_2}$, $\mathrm{CH_4}$, $\mathrm{CO_2}$, $\mathrm{C_2H_4}$, $\mathrm{C_2H_6}$ at 35 °C and pressures up to 30 atm are reported for $6\mathrm{FDA}_{0.5}\text{-}\mathrm{DAPI}_{0.5}$, linear $6\mathrm{FDA}_{0.5}\text{-}\mathrm{DAPI}_{0.33}/\mathrm{DABA}_{0.17}$, and thermally cross-linked $6\mathrm{FDA}_{0.5}\text{-}\mathrm{DAPI}_{0.33}/\mathrm{DABA}_{0.17}$. To further understand structure-property relationships of DAPI-containing polyimides and thermal cross-linking, the performance of the three polymers investigated in this work are compared to Matrimid*, $6\mathrm{FDA}_{0.5}\text{-}\mathrm{DAM}_{0.35}$, linear $6\mathrm{FDA}_{0.5}\text{-}\mathrm{DAM}_{0.33}/\mathrm{DABA}_{0.17}$, and $6\mathrm{FDA}_{0.5}\text{-}\mathrm{DAM}_{0.33}/\mathrm{DABA}_{0.17}$ cross-linked at 389 °C for 40 min. An analysis of pure gas solubility, diffusivity, and $\mathrm{C_2H_4/C_2H_6}$ mixed gas permeability is presented elsewhere [25,26].

For the remainder of this study $6\mathrm{FDA}_{0.5}\text{-DAPI}_{0.33}/\mathrm{DABA}_{0.17}$ and $6\mathrm{FDA}_{0.5}\text{-DAM}_{0.33}/\mathrm{DABA}_{0.17}$ cross-linked for 40 min will be referred to as $6\mathrm{FDA}$ -DAPI/DABA(40 min) and $6\mathrm{FDA}$ -DAM/DABA(40 min), respectively, for brevity. $6\mathrm{FDA}$ -DAPI/DABA and $6\mathrm{FDA}$ -DAM/DABA were cross-linked at $15\,^{\circ}\mathrm{C}$ above their respective glass transition temperatures, unless otherwise specified. Additionally, $6\mathrm{FDA}_{0.5}\text{-DAPI}_{0.5}$ and $6\mathrm{FDA}_{0.5}\text{-DAM}_{0.5}$ will be referred to as $6\mathrm{FDA}$ -DAPI and $6\mathrm{FDA}$ -DAM.

2. Experimental

2.1. Materials

Ethanol, triethylamine (TEA), n-methyl-2-pyrrolidone (NMP), o-dichlorobenzene (o-DCB), and acetic anhydride were used as-received from Sigma Aldrich. Methanol, $\geq 99.8\%$ ACS grade, was used as-received from BDH Chemicals. Hexafluoroisopropylidene diphthalic anhydride (6FDA) was purchased from Alfa Aesar and dried at 200 °C for 6 h under partial vacuum, then held at 150 °C under full vacuum overnight to cyclize any residual diacid moieties. Diaminophenylindane (DAPI) was provided by Dottikon Exclusive Synthesis (Dottikon, Switzerland) and dried at 60 °C under full vacuum overnight. Diaminobenzoic acid (DABA) was purchased from Sigma Aldrich and dried at 150 °C under full vacuum overnight.

2.2. Polymer synthesis

6FDA-DAPI was synthesized via an ester-acid route presented in Scheme 1 [4,5]. A three-neck flask fitted with a Dean-Stark trap, a

Scheme 1. 6FDA-DAPI ester acid synthesis route.

condenser, a mechanical stirrer, and a nitrogen inlet was used as the reaction vessel. 6FDA (10.0 mmol, 4.4424 g), excess ethanol (1200 mmol, 70 mL), and excess TEA (40 mmol, 5.3 mL) were reacted under reflux conditions for 1 h to form the ester-acid of the dianhydride. Excess ethanol and TEA were distilled, leaving a viscous esteracid solution in the reaction vessel. The diamine, DAPI (10.2 mmol, 2.7170 g), was added in slight molar excess to account for slight impurities in the monomer. NMP (50 mL) and o-DCB (10 mL) were added to achieve 10 wt% solids, and the Dean-Stark trap was filled with the azeotroping solvent, o-DCB. To synthesize the polyimide, the solution was held at 180 °C for 24 h, forming a viscous solution. After cooling, the solution was precipitated into methanol while stirring, vacuum filtered, soaked in fresh methanol overnight to remove any residual solvent, and then vacuum filtered again. The resulting powder was dried at 180 °C under vacuum for 24 h.

6FDA-DAPI/DABA was synthesized via chemical imidization, as shown in Scheme 2. Chemical imidization was used to minimize the temperature needed to form the polyimide and prevent potential reaction of the carboxylic acid moiety on DABA during imidization. DAPI (6.66 mmol, 1.7758 g), DABA (3.33 mmol, 0.5072 g), and NMP (16 mL) were added to a three-neck flask fitted with a Dean-Stark trap, a condenser, a mechanical stirrer, and a nitrogen inlet. After the diamines completely dissolved, the reaction flask was placed in an ice bath. Then, 6FDA (10.00 mmol, 4.4424 g) was slowly added over 2 h, and additional NMP (10 mL) was added to bring the solution to 20 wt% solids. Over 24 h, the reaction mixture rose back to room temperature, and the polyamic acid was formed. To cyclize the polyamic acid, acetic anhydride (60 mmol, 5.7 mL) and TEA (60 mmol, 8.4 mL) were added along with additional NMP to bring the solution to 10 wt% solids. The solution was heated to 60 °C for 24 h, cooled to room temperature, and precipitated in methanol while stirring. After vacuum filtration, soaking in fresh methanol overnight, and vacuum filtering again, the resulting polymer powder was vacuum filtered and dried at 180 °C under vacuum for 24 h. Based on previous studies, 6FDA-DAPI/DABA is believed to be

Scheme 2. 6FDA-DAPI/DABA chemical imidization synthetic route.

a random co-polymer [14-16,23,24,27].

2.3. Film casting

Dense polymer films 15–25 μm thick were formed by dissolving the polyimides in tetrahydrofuran (THF, Sigma Aldrich, anhydrous) to prepare a 2 wt% solution. Particulates were removed by filtering the solution through a 1.2 μm Titan3 $^{\text{TM}}$ GMF syringe filter, and the solution was cast onto a glass plate inside a THF saturated glove bag to slow solvent evaporation. After solvent evaporation, the dense polymer film was removed from the glass plate, and residual solvent was removed by heating the sample to 220 $^{\circ}\text{C}$ under full vacuum for 24 h. Solvent removal was confirmed using thermogravimetric analysis, and no mass loss was observed prior to that associated with thermal decarboxylation.

2.4. Characterization

The chemical structure of the linear polyimides were confirmed using solution ^1H NMR and $^1\text{H}\text{-}^1\text{H}$ COSY NMR spectroscopy using an Agilent MR 400 MHz spectrometer and Varian Mercury 400 MHz, respectively. For these studies, a polymer sample was dissolved in tetrahydrofuran-d8 (Sigma-Aldrich, $\geq 99.5\%$) to prepare a 5 wt% solution. Due to the insolubility of the cross-linked polymer, solid-state ^{13}C CP/TOSS NMR measurements with total suppression of spinning side bands were performed using a Bruker AVANCE III HD 400 MHz instrument. A 4 mm H/X cross-polarization magic-angle spinning (CP-MAS) probe was used for these experiments. Approximately equal masses of the linear and cross-linked co-polymer powdered samples were used so a direct comparison could be drawn between structures.

Size exclusion chromatography (SEC) results were collected on a custom Agilent system (Santa Clara, CA) with a 1260 Infinity isocractic pump, degasser, and thermostated column chamber held at 30 °C. The chamber contained Agilent PLgel 10 μm MIXED-B and 5 μm MIXED-C columns with a combined operating range of 200–10,000,000 g/mol

relative to polystyrene standards. Tetrahydrofuran flowing at 0.5 mL/min was used as the mobile phase. Measurement of polymer concentration, molecular weight, and viscosity were provided by a suite of detectors from Wyatt Technologies (Santa Barbara, CA) connected to the effluent of the SEC columns. For molecular weight determination, static light scattering was measured using a DAWN HELEOS II Peltier system. Differential refractive index was measured with an Optilab TrEX, and differential viscosity was measured using a Viscostar II. Refractive index increments (dn/dc) were measured with an Optilab TrEX refractometer.

A Xenocs Ganesha small angle scattering instrument fitted with a moveable Dectris 300k detector was used to conduct wide angle x-ray scattering (WAXS) experiments. The instrument has a microfocus Cu k-alpha source operated at 50 kV and 0.6 mA. Data were corrected for incident beam strength by measuring $I_{\rm o}$ directly on the Dectris detector and for sample thickness to give absolute scattering intensities. A manufacturer supplied software utility, SAXSGUI (Rigaku Innovative Technologies, Inc. and JJ X-Ray Systems ApS) was used to make these corrections and reduced the 2D detector data to intensity versus scattering angle.

A Thermo Nicolet Nexus 470 ESP. Fourier transform infrared spectrometer (FT-IR) was used to characterize the polyimide films. FT-IR was conducted in transmission mode at a spectral resolution of $4\,\mathrm{cm}^{-1}$, and 256 scans were collected for each spectrum.

Thermal stability and mass loss associated with thermal crosslinking were monitored using a TA Instruments Q500 thermogravimetric analyzer coupled with a Thermostar GSD 320 mass spectrometer (TGA-MS). TGA-MS scans were conducted under nitrogen (Airgas, 99.999%, 60 mL/min) between 40 and 800 °C using a 5 °C/min heating rate.

Glass transition temperatures (T_g) were estimated from the first, second, and third scans using a TA Instruments Q100 differential scanning calorimeter (DSC). The DSC samples were heated at 10 $^{\circ}\text{C/min}$ from 25 to 400 $^{\circ}\text{C}$ under nitrogen (Airgas, 99.999%, 50 mL/min). T_g values are reported as the midpoint of the step change in heat capacity for each of the scans.

Scheme 3. Potential cross-linking mechanisms for DABA moieties through thermal decarboxylation of 6FDA-DAPI/DABA [14,15,17].

Density was determined by Archimedes' principle using a density measurement kit (Mettler-Toledo GmbH, P706039, Columbus, OH) and a Mettler-Toledo Balance (ME-T Analytical Balance, Columbus, OH). The buoyant liquid used for the measurement was n-heptane (Sigma, > 99%); the total n-heptane uptake in the samples was negligible, < 0.5% by weight. Eight separate measurements were made for each sample, and the propagation of errors method was used to estimate the uncertainty in density values [28].

2.5. Thermal cross-linking

Polyimide films were cross-linked by thermal decarboxylation, which is reported to proceed according to the mechanism shown in Scheme 3 [14,15,17]. To cross-link a film, it was heated in a tube furnace under a flow of N_2 (~90 cm³/min) at a rate of 40 °C/min to 15 °C above the glass transition temperature of the cross-linked film, held for 10–40 min, and then rapidly quenched by quickly removing the sample from the furnace and cooling to room temperature. To prevent curling, samples were placed between two ceramic plates in the tube furnace. As the DABA-containing polyimide underwent cross-linking, its mass decreased. To quantify the conversion to the cross-linked structure, the degree of cross-linking was defined according to Eq. (1).

$$\% XL = \frac{Actual \ Mass \ Loss}{Theoretical \ Mass \ Loss} x \ 100 \tag{1}$$

The "Actual Mass Loss" is the mass loss observed by weighing the sample before and after the thermal treatment described above, and the "Theoretical Mass Loss" is the mass loss expected if the reaction shown in Scheme 3 were to proceed to completion. Gel fractions were determined using a Soxhlet extractor (Wilmad-LabGlass, P/N LG-6900-100) with THF as the solvent. Samples were refluxed in THF for 24 h, or until the sample was fully dissolved. After drying at 220 °C for 24 h, the gel fraction was calculated by dividing the final dry mass after solvent exposure by the initial sample mass.

2.6. Pure gas permeability and selectivity

Pure gas permeabilities of H_2 , CH_4 , N_2 , O_2 , CO_2 , C_2H_4 , and C_2H_6 were measured at 35 °C over a pressure range of 3–45 atm using a constant volume, variable pressure method [29]. Permeability of species i, P_i , is defined as the pseudo-steady state molar flux of gas, J_i , through the film normalized by the partial pressure difference across the film, Δp_i , and the film thickness, ℓ :

$$P_i = \frac{J_i \ell}{\Delta p_i} \tag{2}$$

For non-ideal gases under high pressure, it is more appropriate to describe the driving force for permeation as the fugacity difference, Δf_i , rather than the partial pressure difference. In this study, fugacity was used to calculate permeability for CO_2 , C_2H_4 , and C_2H_6 . The fugacity coefficients for pure gases were calculated using the NIST Reference Fluid Thermodynamic and Transport Properties Database (REFPROP) as described in the Supporting Information (SI) [30]. Permeability coefficients are reported in Barrer, where 1 Barrer = 10^{-10} cm³(STP) · cm/(s cm² · cmHg). Ideal selectivity between two gases, i and j, is defined as the ratio of their pure gas permeabilities [29]:

$$\alpha_{i/j} = \frac{P_i}{P_j} \tag{3}$$

For this study, each gas was tested at the same pressure points, and each pressure point was held for 6 times the time lag while the downstream was held near vacuum (< 10 Torr) for the entire test [29]. The gases were tested in the previously mentioned order, and a new sample was used after exposure to $\rm CO_2$, $\rm C_2H_4$, and $\rm C_2H_6$. To check reproducibility, $\rm H_2$ was measured on each new sample to ensure transport properties were consistent among samples of the same material. Additional details regarding sample preparation and permeation equipment are recorded in the SI.

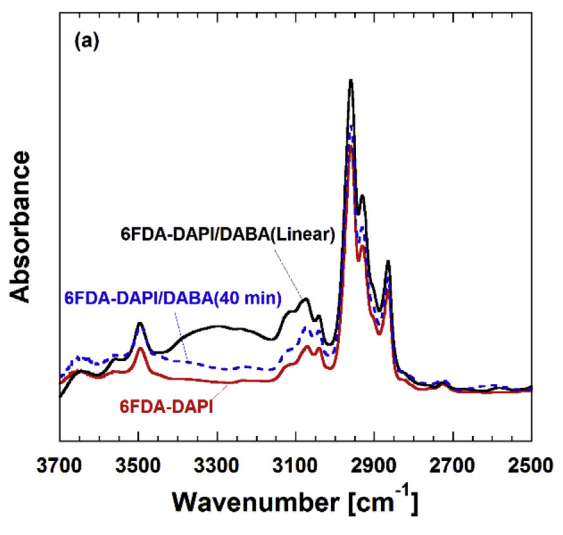
3. Results and discussion

3.1. Polymer structure

The molecular weights and molecular weight distributions of the linear polyimides were determined by SEC and are presented in Table S2 of the SI. The molecular weights of all samples were sufficiently high to form mechanically robust free standing films. The structures and complete imidization of these polymers were confirmed by NMR and FTIR, as explained in more detail in the SI.

The cross-linking mechanism was investigated via transmission mode FT-IR [14-16]. The spectra for linear 6FDA-DAPI, linear 6FDA-DAPI/DABA, and 6FDA-DAPI/DABA(40 min), normalized to the imide ring deformation at 720 cm⁻¹, are included in Fig. 1-a. More complete FT-IR results are presented in the SI. After cross-linking, the broad peak between 3100 and 3500 ${\rm cm}^{-1}$ associated with the carboxylic acid –OH stretch decreased nearly to the same absorbance observed for 6FDA-DAPI, indicating that disappearance of these groups is due to the thermal treatment [15,17]. After equilibrating with ambient air, the content of both 6FDA-DAPI/DABA and 6FDA-DAPI/ DABA(40 min) films were ca. 0.25 wt%, based on TGA. The low and similar water contents in both films suggest that the change in the broad peak between 3100 and 3500 cm⁻¹ is due to a structural change between the cross-linked and linear samples, not simply differences in the amount of water absorbed by the samples. Additionally, as shown in Fig. 1-b, a double peak at 1720 cm⁻¹ was observed for linear 6FDA-DAPI/DABA, and after cross-linking at 353 °C for 40 min, only a single peak was observed. This additional peak was likely associated with the carboxylic acid group in the DABA monomer unit. The disappearance of this peak after heating is consistent with the loss of the DABA carboxylic acid groups in the cross-linked structure, which is consistent with the cross-linking mechanisms presented in Scheme 3 and other reports for similar structures [15,17].

Once the polyimide films were cast and dried, TGA-MS and DSC were used to confirm complete solvent removal and to investigate thermal properties. TGA measurements coupled with mass spectroscopy of the evolved gases were conducted to characterize the thermal decarboxylation and decomposition of the polymers. Fig. 2-a shows the mass loss and derivative mass loss of 6FDA-DAPI and linear 6FDA-DAPI/DABA. For both polymers, no significant mass loss was observed



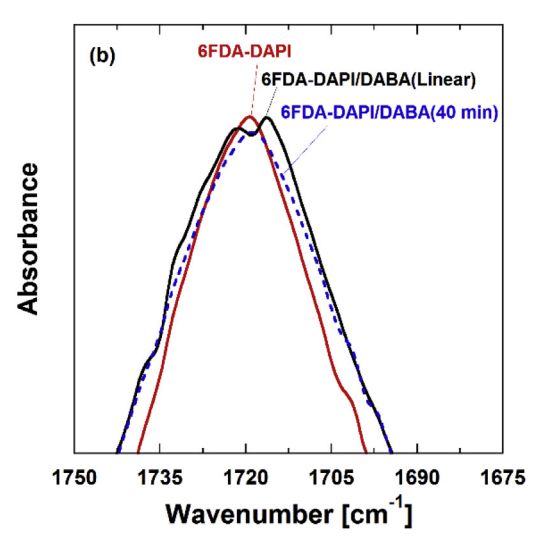


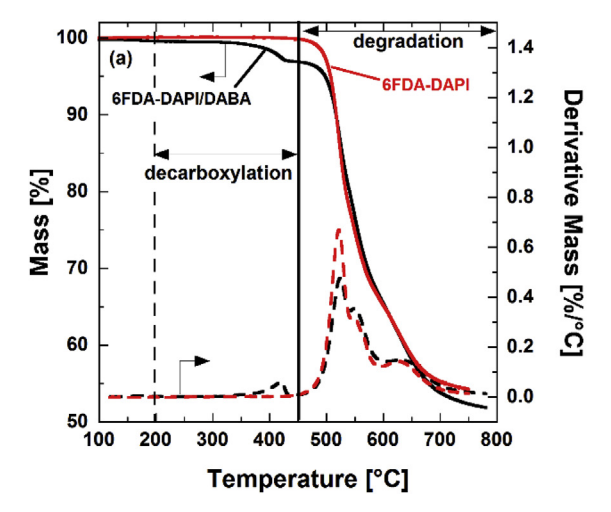
Fig. 1. (a) High frequency range of the transmission FTIR spectra of 6FDA-DAPI [red], linear 6FDA-DAPI/DABA [black], and 6FDA-DAPI/DABA(40 min) [blue]. (b) Carbonyl stretch, showing the additional peak at 1717 cm⁻¹ associated with the carboxylic acid group in DABA for linear 6FDA-DAPI/DABA. (For interpretation of the references to colour in this figure legend, the reader is referred to the Web version of this article.)

below 200 °C, indicating no residual solvent remained in the cast films. Linear 6FDA-DAPI/DABA exhibited two distinct mass loss regions, a smaller loss starting at about 200 °C and a larger mass loss starting at 450 °C. The lower temperature mass loss is attributed to thermal decarboxylation of the DABA moieties (cf. Scheme 3), and the higher temperature mass loss is attributed to thermal degradation of the polymer backbone. This conclusion is supported by TGA-MS of linear 6FDA-DAPI/DABA, reported in Fig. 2-b, where a peak in the atomic mass intensities for CO_2 (m/z = 44) correlated with the lower temperature mass loss region and a peak in degradation products, such as CF_3 (m/z = 69), correlated with the higher temperature mass loss [31]. The atomic mass intensities for H_2O (m/z = 18), reported in Figure S5, correlated with both the lower temperature and the higher temperature mass loss regions, suggesting H₂O is likely a product of both the thermal decarboxylation as well as the thermal degradation. Furthermore, 6FDA-DAPI exhibited only one mass loss region, starting at about 450 °C, which is attributed to thermal degradation of the polymer backbone. While some cross-linking mechanisms indicate the evolution of H2O, CO2, and CO during decarboxylation of pendent -COOH groups, CO (m/z = 28) could not be detected since its molecular mass

overlapped that of the N_2 sweep gas (m/z = 28) [14–17].

The glass transition temperature, T_g , of 6FDA-DAPI was 322 °C, defined as the mid-point of the step change in heat capacity during the second DSC heating scan (cf., Fig. 3). For linear 6FDA-DAPI/DABA, several features, including a broad endothermic band from 270 to 380 °C, were observed on the first scan, and no clear glass transition temperature was observed. While the small thermal event around 240 °C could be due to decarboxylation, poor contact with the sample pan, or sample processing history, the broad endothermic peak occurs in the same temperature range as the large peak in the mass spectrometry signal for CO_2 (cf., Fig. 2-b). The broad endothermic peak is ascribed to decarboxylation of the DABA moieties. On the second scan, only a glass transition was observed, at 338 °C, and it increased slightly on subsequent scans, consistent with most of the DABA undergoing decarboxylation during the first heating cycle.

Compared to Matrimid $^{\circ}$ (T_g = 310 $^{\circ}$ C [32]), 6FDA-DAPI has a higher glass transition temperature, consistent with the $-C(CF_3)_2$ – linkages contributing to a higher T_g relative to the benzophenone linkages in BTDA in Matrimid $^{\circ}$. As observed with similar polymers, polymer chain mobility was potentially reduced slightly when DABA and cross-



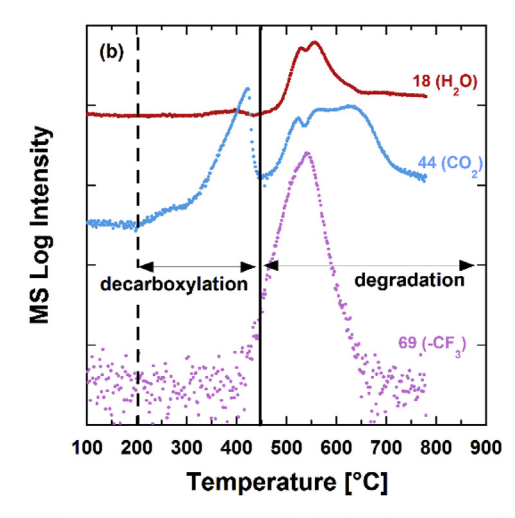


Fig. 2. (a) TGA mass loss and derivative mass loss with temperature of 6FDA-DAPI [red] and linear 6FDA-DAPI/DABA [black] (b) The corresponding mass spectrometry signal from the evolved gases of linear 6FDA-DAPI/DABA during TGA for H_2O (mz = 18, red), CO_2 (mz = 44, blue), and CF_3 (mz = 69, pink). The mass spectrometry signal for H_2O is also reported separately in Figure S5 of the SI. (For interpretation of the references to colour in this figure legend, the reader is referred to the Web version of this article.)

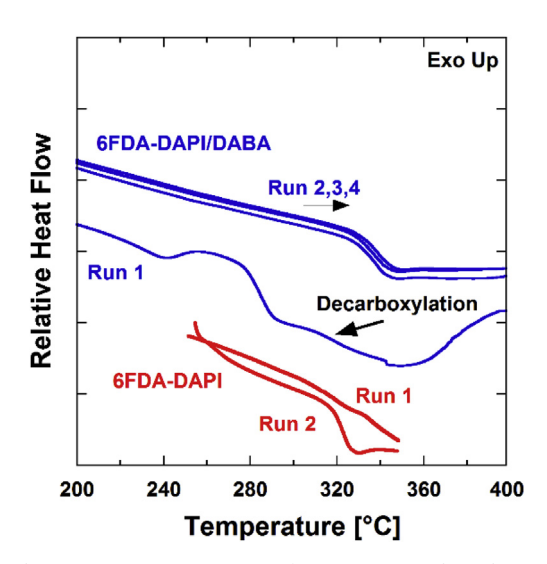


Fig. 3. Glass transition temperatures of 6FDA-DAPI [red] and 6FDA-DAPI/DABA [blue], linear and cross-linked at 353 °C for 40 min, determined by DSC. (For interpretation of the references to colour in this figure legend, the reader is referred to the Web version of this article.)

linking were introduced in 6FDA-DAPI/DABA [14,15,17]. 6FDA-DAM and cross-linked 6FDA-DAM/DABA(40 min) have T_g values of 372 °C and 376 °C, respectively [33]. Thus, DAPI incorporation reduces T_g relative to DAM incorporation in these polymers.

3.2. Polymer cross-linking

As mentioned above, DABA decarboxylation was assessed by measuring the mass loss associated with the lower temperature mass loss region (200–440 °C) in the TGA scan of linear 6FDA-DAPI/DABA (cf. Fig. 2-a). This mass loss was 2.40%, which is slightly greater than the expected theoretical mass loss of 2.36%, assuming 100% decarboxylation according to the mechanism in Scheme 3. Due to the separation between thermal decarboxylation (200–440 °C) and thermal degradation (> 450 °C), 6FDA-DAPI/DABA appears to be cross-linked prior to the onset of significant thermal degradation. For this study, a cross-linking temperature of 353 °C, 15 °C above the measured $T_{\rm g}$ of the cross-linked polymer but below the onset of large scale degradation, was selected. While others [14,15,17] have demonstrated cross-linking of similar materials below $T_{\rm g}$, we used a temperature above $T_{\rm g}$ to favor rapid and near theoretical conversion to the cross-linked structure, since rapid polymer chain motion would facilitate cross-linking.

To prepare cross-linked samples for further study, the heating protocol detailed in Figure S1 of the SI was followed. In this protocol, samples were heated in a tube furnace under a $\rm N_2$ atmosphere at a ramp rate of 40 °C/min from ambient to 353 °C and held for 10, 20, or 40 min at 353 °C before being rapidly quenched to room temperature. The observed mass loss, theoretical conversion, gel fraction, and measured density of each thermally treated sample are recorded in Table 1.

As cross-linking time increased from 10 to 40 min, the theoretical conversion of 6FDA-DAPI/DABA to the cross-linked structure increased from 32.2% to 103%, respectively. The 3% excess mass loss observed for the 40 min cross-linked sample may be due to water loss and/or a small amount of thermal degradation occurring during the longest thermal treatment time considered. Similarly, gel fraction increased with theoretical conversion, with the 10 min treated sample remaining fully soluble in hot THF. The 20 min and 40 min samples had gel fractions of 93.9% and 97.2%, respectively. While the 10 min sample remained soluble, it may be partially cross-linked with a cross-link density lower than that needed to form an insoluble network [34].

Thermally treating linear 6FDA-DAPI at 353 °C for 40 min resulted in a gel fraction of 30.1%, despite the absence of carboxylic acid groups for cross-linking. The fact that the linear polymer is partially insoluble may be due to the thermal treatment increasing inter-chain charge transfer complexes which have been shown to decrease solubility of aromatic polyimides [17,35,36]. Thus, the increase in gel fraction with increasing thermal treatment time appears to derive from both cross-linking via the DABA units as well as other mechanisms, such as formation of charge transfer complexes.

The linear and cross-linked films were tested for solubility in chloroform (CHCl₃), dichoromethane (CH₂Cl₂), tetrahydrofuran (THF), toluene, *N*-methyl-2-pyrrolidinone (NMP), and *N*,*N*-dimethylacetamide (DMAc). As shown in Table S3 in the SI, 6FDA-DAPI was soluble in all solvents considered, and linear 6FDA-DAPI/DABA was soluble in THF, NMP, and DMAc. The 6FDA-DAPI/DABA(40 min) cross-linked sample did not dissolve in any of the solvents considered and showed no visual signs of swelling or deformation when boiled in NMP or DMAc.

3.3. Polymer density, fractional free volume (FFV), and cross-linking route

Based on previous studies, the two most likely cross-linking methods are radical combination (Route d in Scheme 3) and/or methyl-hydrogen abstraction (Routes a and b in Scheme 3). While it is possible for the radicals generated by carboxylic acid decomposition to abstract hydrogens from other locations on the polymer backbone or to react with the fluorine groups in 6FDA, these reaction pathways are structurally hindered or require higher activation energies [15-17,37]. To better identify the potential cross-linking mechanism, and due to the insolubility of cross-linked samples, ¹³C CP/TOSS solid-state NMR measurements were performed on the linear and the most cross-linked (353 °C, 40 min) samples. The results are presented in Fig. 4 with the labeled peaks corresponding to the carbons in the structure. After crosslinking, only a slight increase in peaks at 140 and 127 ppm, associated with aromatic carbons, was observed. Additionally, no significant change in the peak at 170 ppm, associated with the C=O groups, after cross-linking was observed, likely due to the overwhelming signal from the imide ring C = O groups, which outnumber the carboxylic acid C = Ogroups 12:1. Additionally, ¹³C CP/TOSS solid-state NMR is less sensitive for carbons which do not have protons. The absence of changes in the peaks associated with -CH₂- and -CH₃ (peaks between 25 and 60 ppm) likely indicates that most cross-linking occurs between two aromatic groups (Route d in Scheme 3), rather than by abstraction of methyl

Mass loss, gel fraction, density, and fractional free volume (FFV) of 6FDA-DAPI and 6FDA-DAPI/DABA cross-linked at 353 °C for 0, 10, 20, 40 min.

Polymer	Thermal Treatment	Mass Loss (%)	Theor. Conv. (%)	Gel Fraction (%)	Density (g/cm ³)	FFV (route d) ^a	FFV (route a & b) ^a
6FDA-DAPI	None	_	_	0	1.296 ± 0.009	0.181 ± 0.003	
	353 °C, 40 min	1.655	_	30 ± 5	_	_	
6FDA-DAPI/DABA	None	_	_	0	1.337 ± 0.008	0.179 ± 0.002	
	353 °C, 10 min	0.761	32.2	0	1.334 ± 0.008	0.180 ± 0.002	0.181 ± 0.002
	353 °C, 20 min	1.37	58.3	93 ± 3	1.333 ± 0.009	0.181 ± 0.002	0.183 ± 0.002
	353 °C, 40 min	2.42	103	97 ± 3	1.338 ± 0.009	0.177 ± 0.002	0.181 ± 0.002

^a Note: FFV was calculated according to Eq. S1 in the SI, using experimental density values and group contribution theory to predict the occupied volume, and Eq. S2, assuming cross-linking occurs by either 100% radical combination (Route *d* in Scheme 3) or 100% methyl hydrogen abstraction (Route *a* and *b* in Scheme 3).

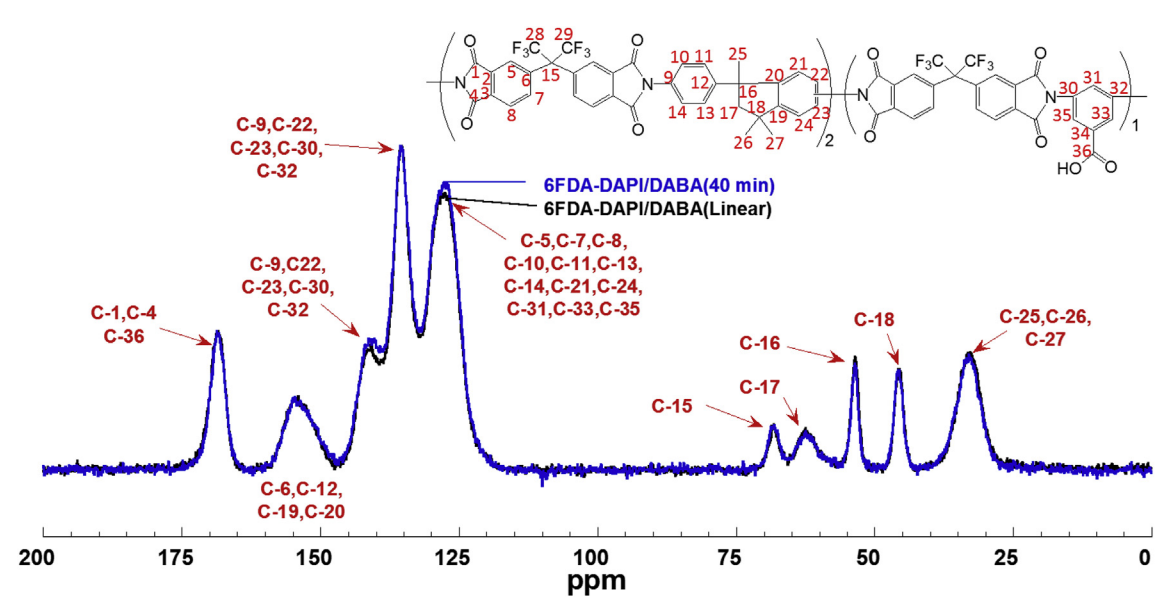


Fig. 4. ¹³C CP/TOSS solid state NMR of linear 6FDA-DAPI/DABA [black] and 6FDA-DAPI/DABA(40 min) [blue]. The data was collected using a 5 s relaxation delay with 2048 total scans. Labeled carbons correspond to carbons in noted structure. (For interpretation of the references to colour in this figure legend, the reader is referred to the Web version of this article.)

hydrogens (Routes a and b in Scheme 3). Cross-linking by Routes a and b may still occur, but the presence of functional groups associated with this mechanism are below the detection limit. To better investigate the cross-linking route by SS-NMR, increasing the quantity of DABA in the copolymer (i.e., using a DAPI:DABA ratio of 1:1 or 1:2, rather than 2:1) is suggested, but this study is beyond the scope of the current investigation.

To estimate the FFV of cross-linked samples, the occupied volume, V_o , was calculated using group contribution theory for Routes a, b, and d. Using group contribution theory, Routes a and b cannot be distinguished, so these reaction pathways have been grouped together for FFV analysis. While it is possible that both cross-linking pathways occur simultaneously, the two routes are considered separately, either solely by radical coupling or solely by methyl hydrogen abstraction, to help identify how each route contributes to the total FFV of the polymer matrix. Fractional free volume was calculated using the methods described in the SI [38], adjusting V_o for each polymer based on the fractional conversion to the cross-linked structure (cf. Eq. S1 and Eq. S2) and using the experimental density values from Table 1.

The density values for 6FDA-DAPI and 6FDA-DAPI/DABA crosslinked at 353 °C for 0, 10, 20, and 40 min are recorded in Table 1 along with the FFV values for the two cross-linking mechanisms. The polar -COOH groups in linear 6FDA-DAPI/DABA likely favor increased hydrogen bonding, producing a more dense polymer matrix than in 6FDA-DAPI. However, the density of 6FDA-DAPI/DABA samples heated at 353 °C for 10, 20, and 40 min remained constant, with any potential differences falling within the experimental uncertainty. According to group contribution theory, there is only a minimal difference in the theoretical occupied volume for the two potential cross-linked structures (Figure S6), which results in no discernible difference in FFV between the two potential cross-linking mechanisms (Table 1 and Fig. S6). The FFV values are not sensitive to the cross-linking routes, and within the experimental uncertainty of the density measurements, no discernible differences in FFV between any of the DAPI-containing polymers in this study were detected.

To further characterize these materials, WAXS was used to probe inter-and intra-polymer chain spacing within the samples. As shown in Fig. 5-a and Fig. S7, two scattering peaks were observed for all polymers, a lower intensity scattering peak around 5°, corresponding to scattering distances of about 17 Å, and a higher intensity scattering

peak around 15°, corresponding to scattering distances of about 5.7 Å. The scattering peak around 15°, reported in Fig. 5-b, is in the same range as other 6FDA containing polyimides [39]. A slight increase in the maximum peak intensity and slight shift in d-spacing were observed as 6FDA-DAPI/DABA cross-linking time increased. Linear 6FDA-DAPI/ DABA and 6FDA-DAPI/DABA(10 min) had a d-spacing of 5.63 Å, while 6FDA-DAPI/DABA(20 min), 6FDA-DAPI/DABA(40 min), and 6FDA-DAPI had d-spacing values of 5.66 Å, 5.73 Å, and 5.76 Å, respectively. Additionally, an increase in absolute scattering intensity was observed, following the same trend as the d-spacing shift, with 6FDA-DAPI having the highest scattering intensity, indicating an increase in structural order with increasing d-spacing. This slight increase in d-spacing qualitatively correlates with the measured gas permeability (as shown below), suggesting there may be a slight increase in FFV with increased cross-linking time, although any change in FFV was too subtle to detect via density-based FFV calculations. This point will be discussed in detail later, and additional WAXS analysis is included in the SI.

Compared to similar polymers, FFV increases in the following order: Matrimid[®] (17.0% 6FDA-DAPI/DABA [32]) < linear $(17.9 \pm 0.02\%) \approx 6$ FDA-DAPI $(18.1 \pm 0.03\%) < linear 6$ FDA-DAM/ DABA (18.3% [33]), < 6FDA-DAM (19.0% [33]). Comparing 6FDA-DAPI to Matrimid®, the -C(CF₃)₂- linkages in 6FDA contributed to a higher FFV than the benzophenone linkages in BTDA. Relative to 6FDA-DAM, FFV decreased when DABA was introduced into 6FDA-DAM/ DABA, suggesting incorporating DABA into the backbone may have facilitated additional hydrogen bonding and reduced FFV. This effect was minimal for the DAPI-containing polyimides in this work, with no detectible change in FFV when DABA was incorporated into the polymer structure. Consistent with the trends in Tg, the rigid, bulky DAM structure gave a higher FFV in 6FDA-DAM and linear 6FDA-DAM/ DABA than DAPI in 6FDA-DAPI and linear 6FDA-DAPI/DABA. The changes in FFV with changes in polymer structure are reflected in pure gas permeability coefficients, as shown in Table S6 in the SI [38].

3.4. Influence of cross-linking on pure gas permeability and selectivity

As presented in Fig. 6-a, Fig. S10, and Fig. S11, all materials show minimal pressure dependence for H_2 , O_2 , N_2 , and CH_4 pure gas permeability coefficients. In contrast, CO_2 , C_2H_4 , and C_2H_6 permeabilities increase at high pressures for some samples. This behavior is typical of

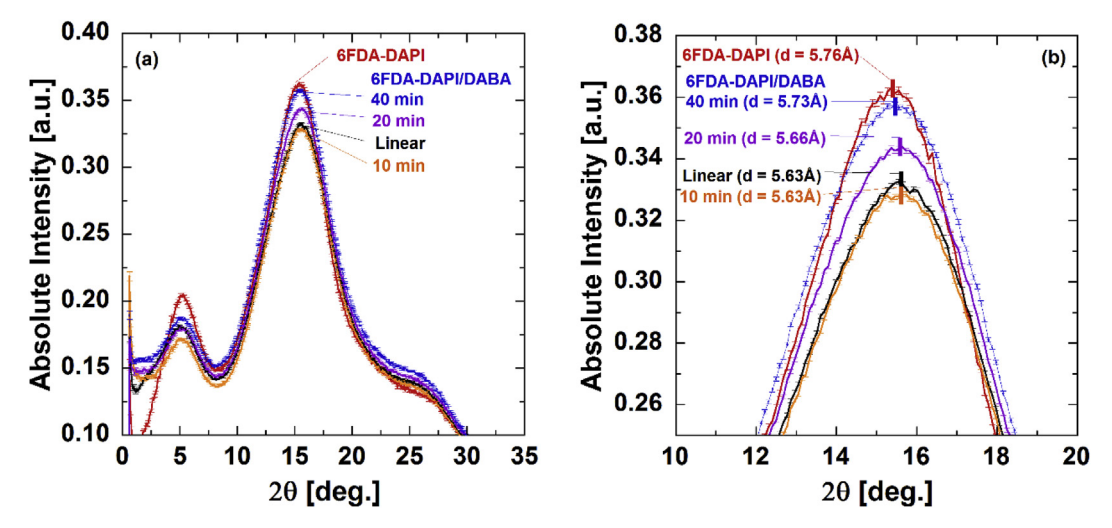


Fig. 5. (a) The full 2θ range of wide angle x-ray scattering of 6FDA-DAPI [red], linear 6FDA-DAPI/DABA [black], and 6FDA-DAPI/DABA(10 min) [orange], 6FDA-DAPI/DABA(20 min) [purple], and 6FDA-DAPI/DABA(40 min) [blue] and (b) the large scatting peak at $10^{\circ} < 2\theta < 20^{\circ}$. The noted d-spacing for each sample were calculated using the 2θ at the maximum scattering intensity of the large peak. (For interpretation of the references to colour in this figure legend, the reader is referred to the Web version of this article.)

gas transport in glassy-polymers, where dual-mode behavior predicts a decrease in permeability at low partial pressure driving force and approaches a constant value at higher pressures [40]. However, highly condensable and strongly sorbing gases, like CO_2 , C_2H_4 , and C_2H_6 , can interact strongly with the polymer and induce plasticization, or swelling, of the polymer matrix, at high pressures. Both linear 6FDA-DAPI/DABA and 6FDA-DAPI/DABA(40 min) showed minimal increase in C_2H_4 and C_2H_6 permeability at high pressures, suggesting potentially improved plasticization resistance compared to 6FDA-DAPI. Plasticization resistance and C_2H_4/C_2H_6 mixed gas permeability of these polymers will be discussed further in a subsequent publication [25,26].

The pure gas permeability data at 5 atm are summarized in Table S6. The ideal selectivity at 5 atm for several relevant gas pairs were calculated using Eq. (3) and are summarized in Table S7. For all polymers, gas permeabilities followed the trend shown in Fig. 6, P $(C_2H_6) < P(CH_4) < P(C_2H_4) < P(N_2) < P(O_2) < P(CO_2) < P(H_2)$, where permeability increased with decreasing gas diameter (Table S6), with CO_2 and C_2H_4 deviating slightly from this trend. This result is

demonstrated in Fig. 6-b, where pure gas permeabilities at 5 atm for 6FDA-DAPI, linear 6FDA-DAPI/DABA, and 6FDA-DAPI/DABA(40 min) are plotted versus gas diameter squared, d_g^2 . This trend is consistent with diffusion controlled gas transport, and the deviation of CO₂ and C₂H₄ is often observed due to their relatively high solubility coefficients in polymers [41].

When comparing the transport properties of 6FDA-DAPI to linear 6FDA-DAPI/DABA, introduction of the DABA moiety decreases permeability for all gases. The percent decrease in permeability was $\rm CO_2$ (50.4%), $\rm C_2H_4$ (46.6%), $\rm C_2H_6$ (41.9%), $\rm CH_4$ (37.1%), $\rm N_2$ (25.9%), $\rm O_2$ (22.6%), and $\rm H_2$ (17.0%). Larger and more condensable gases exhibited a larger decrease in permeability than smaller, less condensable species. Additionally, the ideal selectivity, for most of the gas pairs summarized in Table S7, increased when DABA was incorporated into the polymer backbone structure.

After thermally treating linear 6FDA-DAPI/DABA for various times, the permeability of all gases increased with increasing conversion to the cross-linked structure (cf., Table S6). The permeability coefficients of

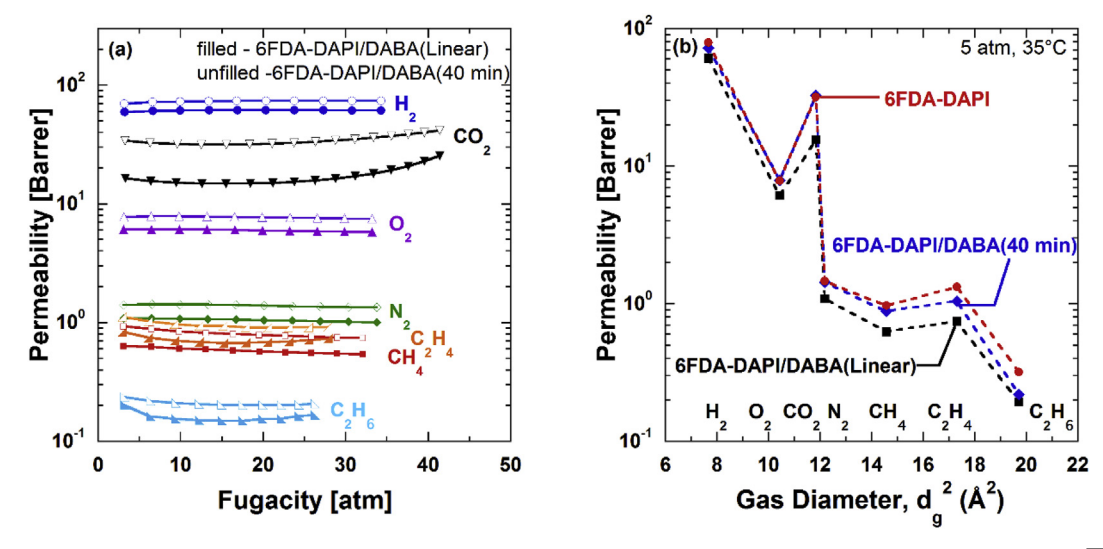


Fig. 6. (a) Pure gas permeability of linear 6FDA-DAPI/DABA [filled markers] and 6FDA-DAPI/DABA(40 min) [unfilled markers] for H_2 [\bullet], C_2 [\blacktriangledown], O_2 [\bullet], O_2 [

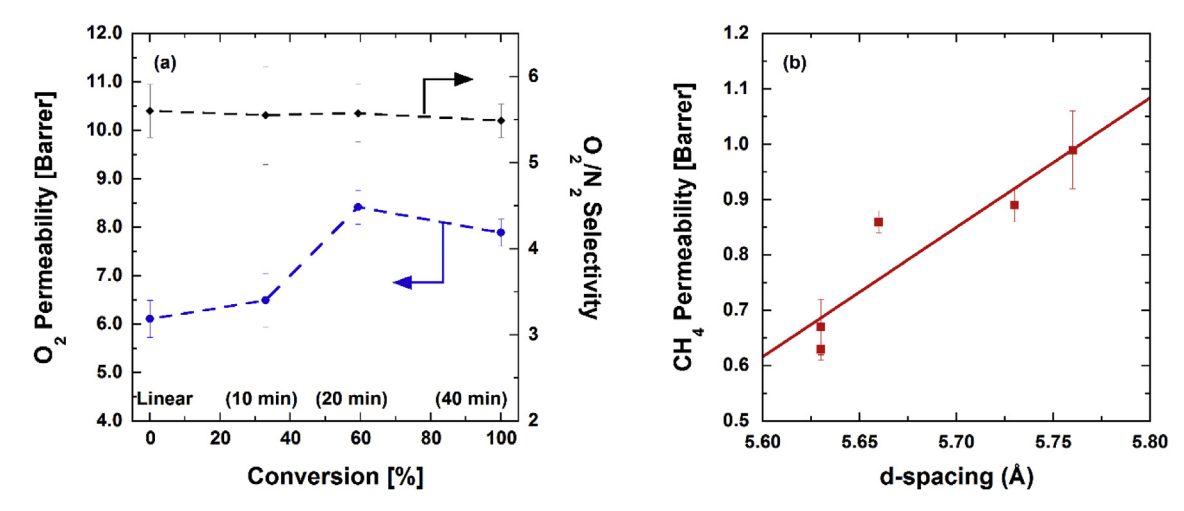


Fig. 7. (a) O_2 permeability [\bullet] and O_2/N_2 selectivity [\bullet] versus theoretical conversion of 6FDA-DAPI/DABA cross-linked at 353 °C, reported at 35 °C and 5 atm. (b) CH₄ permeability (\bullet) at 5 atm and 35 °C versus inter-chain d-spacing of DAPI-containing polyimides (cf., Table S5) measured by WAXS.

linear 6FDA-DAPI/DABA and 6FDA-DAPI/DABA(40 min) are plotted versus fugacity in Fig. 6-a. As conversion increased from the linear structure to the fully crosslinked structure (353 °C, 40 min), the permeability of each gas increased as follows: H_2 (18.8%) $< C_2H_6$ $(13.3\%) < O_2$ $(29.1\%) < N_2$ $(31.8\%) < C_2H_4$ $(39.3\%) < CH_4$ (41.4%) < CO₂ (109%). The ideal selectivity remained relatively constant as conversion increased (cf., Table S7). An example of this trend can be observed in Fig. 7-a, where O2 permeability increased by 30% as cross-linking time increased from 0 min to 40 min, and O₂/N₂ ideal selectivity was generally independent of conversion. Due to the larger increase in CO₂ permeability than other gases upon cross-linking, pure gas selectivity for gas pairs including CO₂ (CO₂/CH₄, CO₂/N₂) increase with increasing conversion (cf. Table S6), with CO₂/CH₄ selectivity increasing by 48% and CO₂/N₂ selectivity increasing by 64% as conversion increased from 0 to 103%. This large increase in CO2 permeability coupled with increases in selectivities, may be due to increased CO2 diffusivity, as judged based on the slight increase in dspacing, which may reflect a slight increase in inter-chain spacing, with cross-linking.

This increase in pure gas permeability with increased thermal treatment time suggests a more open polymer matrix after cross-linking. In many cases, cross-linking a polymer significantly decreases its permeability due to a reduction in FFV and reduced segmental chain motion that permits slower diffusion [43,44]. In our case, there was no observable difference in FFV upon cross-linking. However, there was a slight increase in inter-chain d-spacing, which did correlate, roughly, with permeability. An example of this correlation is shown in Fig. 7-b for CH₄ and for other gases in Figs. S12 and S13. By cross-linking above Tg, the polymer chains may organize to a slightly higher, though undetectable, FFV, which is trapped upon cross-linking and quenching to ambient temperature. To confirm that the higher gas permeability was long-lived, 6FDA-DAPI/DABA(40 min) was held at 220 °C for 24 h under vacuum, which might be expected to relax any highly nonequilibrium excess free volume [45,46]. As shown in Fig. 8 for CH₄, the aged, cross-linked sample had slightly higher pure gas permeabilities than the cross-linked sample, so any changes in free volume were not short-lived. This indicates any additional free volume incorporated into the matrix during the cross-linking process is likely permanent.

3.5. Pure gas selectivity

The C_2H_4/C_2H_6 and CO_2/CH_4 pure gas selectivities are presented in Fig. 9 on upper bound plots for 6FDA-DAPI, linear 6FDA-DAPI/DABA, and 6FDA-DAPI/DABA(40 min). As is evident in the C_2H_4/C_2H_6 upper bound plot, the permeability of C_2H_4 in linear 6FDA-DAPI/DABA is

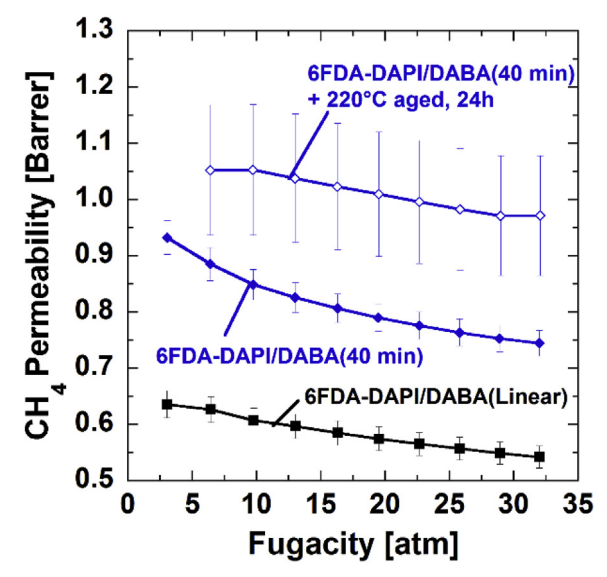
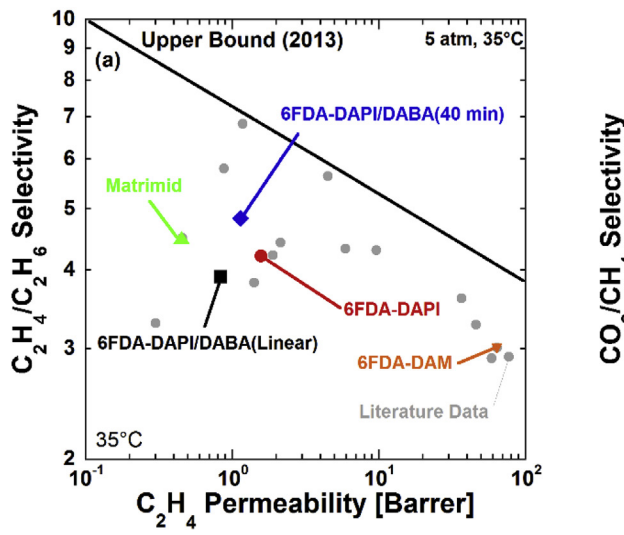


Fig. 8. CH_4 pure gas permeability in linear 6FDA-DAPI/DABA [\blacksquare], 6FDA-DAPI/DABA(40 min) [\blacklozenge], and 6FDA-DAPI/DABA(40 min) aged at 220 °C for 24h [\diamondsuit]. Permeation results for other gases in "aged" cross-linked 6FDA-DAPI/DABA are included in Fig. S14 of the SI.

lower than that of 6FDA-DAPI and only a minimal decrease in selectivity is observed. After cross-linking 6FDA-DAPI/DABA, both pure gas permeability and selectivity increased. The increase in permeability is consistent with the cross-linked polymer having a more open structure than both linear polymers, and the increase in selectivity is likely due to increased size sieving in the cross-linked polymer matrix (cf., Fig. 5 and Section 3.3 discussing the density and FFV analysis). These results will be investigated further in a subsequent publication reporting pure gas solubility and diffusivity data in these polymers as well as mixed gas permeation properties with an equal molar feed gas mixture of C_2H_4 : C_2H_6 [25,26].

For the $\rm CO_2/CH_4$ gas pair, both pure gas permeability and selectivity were lower in linear 6FDA-DAPI than in linear 6FDA-DAPI/DABA. The decrease in selectivity for this particular gas pair is due to a stronger Langmuir-type decrease in $\rm CO_2$ permeability than for $\rm CH_4$, resulting in an apparent decrease in selectivity (cf., Fig. 6-a and Fig. S10). After fully cross-linking 6FDA-DAPI/DABA, both permeability and selectivity increased, resulting in similar values to those of linear 6FDA-DAPI.



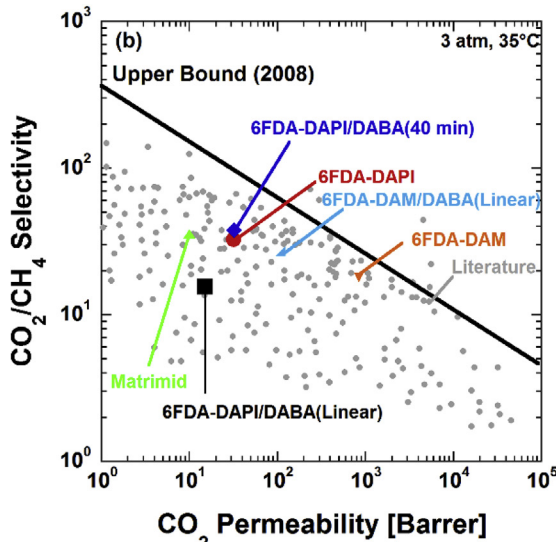


Fig. 9. Upper bound plots for: (a) C_2H_4/C_2H_6 at 5 atm [13] and (b) CO_2/CH_4 at 3 atm [20] for 6FDA-DAPI [\bullet], linear 6FDA-DAPI/DABA [\blacksquare],6FDA-DAPI/DABA(40 min) [\bullet], data collected from literature [\bullet] [13]. Matrimid * [Δ] properties for C_2H_4/C_2H_6 (3.4 atm) and CO_2/CH_4 (4 atm) were obtained from Refs. [13,47], respectively [48]. Pressures for literature points vary slightly. 6FDA-DAM [\blacktriangledown] [33,49,50] and linear 6FDA-DAM/DABA [Δ] [33,51] data are from the literature.

4. Conclusions

6FDA-DAPI/DABA was cross-linked by thermal decarboxylation of DABA. The cross-linking mechanism was investigated by DSC, TGA-MS, FTIR, and ¹³C CP/TOSS solid state NMR, revealing removal of the carboxylic acid group during the thermal treatment. No detectable change in FFV due to cross-linking was detected using experimental density values. However, WAXS revealed a slight increase in inter-chain d-spacing after thermal cross-linking, qualitatively trending with the observed increase in gas permeability in the cross-linked samples. As cross-linking conversion increased, pure gas permeability increased, with 6FDA-DAPI/DABA(40 min) having 30% higher pure gas permeability for most gases, with no significant loss in ideal selectivity relative to its uncross-linked analog. Compared to Matrimid*, the 6FDA unit increased gas permeability in 6FDA-DAPI and linear 6FDA-DAPI/DABA and 6FDA-DAPI/DABA(40 min).

Acknowledgments

This material is based upon work supported in part by the National Science Foundation Graduate Research Fellowship under Grant No. DGE-1610403. The authors gratefully acknowledge partial support from the Division of Chemical Sciences, Geosciences, and Biosciences, Office of Basic Energy Sciences of the U.S. Department of Energy (DOE), USA through Grant DE-FG02-02ER15362 for the synthesis and characterization studies. Additionally, BDF's work in preparing this manuscript was supported in part by the National Science Foundation under Cooperative Agreement No. EEC-1647722. Any opinions, findings and conclusions or recommendations expressed in this material are those of the authors and do not necessarily reflect the views of the National Science Foundation. NAL and MC thank the National Science Foundation for partial support of this research (CBET-1706968), specifically for the NMR and molecular weight analysis. Use of the ¹³C CP/ TOSS solid-state NMR instrumentation is funded in part by NSF grant No. CHE-1623211. The authors acknowledge Steve Swinnea and Steve Sorey from The University of Texas at Austin for their assistance in measuring and interpreting WAXS and SS-NMR results, respectively.

Appendix A. Supplementary data

Supplementary data to this article can be found online at https://

doi.org/10.1016/j.polymer.2018.11.050.

References

- [1] R.W. Baker, Future directions of membrane gas separation Technology, Ind. Eng. Chem. Res. 41 (2002) 1393–1411.
- [2] R.W. Baker, Membrane Technology and applications, Membrane Technology, John Wiley & Sons, Ltd, Chichester, UK, 2004, p. 545.
- [3] S.A. Stern, Polymers for gas separationis: the next decade, J. Membr. Sci. 94 (1994)
- [4] I.V. Farr, Synthesis and Characterization of Novel Polyimide Gas Separation Membrane Material Systems, PhD Dissertation Virginia Polytechnic Institute and State University, 1999.
- [5] I.V. Farr, D. Kratzner, T.E. Glass, D. Dunson, Q. Ji, J.E. McGrath, The synthesis and characterization of polyimide homopolymers based on 5(6)-amino-1-(4-aminophenyl)1,3,3-trimethylindane, J. Polym. Sci. Polym. Chem. 38 (2000) 2840–2854.
- [6] T. Visser, M. Wessling, Auto and mutual plasticization in single and mixed gas C3 transport through matrimid-based hollow fiber membranes, J. Membr. Sci. 312 (2008) 84–96.
- [7] Z.P. Smith, Fundamentals of Gas Sorption and Transport in Thermally Rearranged Polyimides, PhD Dissertation The University of Texas at Austin, Austin, TX, 2014.
- [8] U.S. Shale Production, U.S. Energy Information Administration, 2018, https://www.eia.gov/dnav/ng/hist/res_epg0_r5302_nus_bcfa.htm.
- [9] Hydrocarbon Gas Liquids Explained, U.S. Energy Information Administration, 2018, https://www.eia.gov/energyexplained/index.php?page=hgls_home.
- [10] R.W. Baker, Membrane Technology and Applications, third ed. ed., A John Wiley & Sons, Ltd., Publication, 2012.
- [11] G.E. Keller, A.E. Marcinkowsky, S.K. Verma, K.D. Williamson, Olefin recovery and purification via silver comlexation, in: N.N. Li, J.M. Calo (Eds.), Separation and Purification Technology, Marcel Dekker, New York, 1992.
- [12] D.J. Safarik, R.B. Eldridge, Olefin/paraffin separations by reactive absorption: a review, Ind. Eng. Chem. Res. 37 (1998) 2571–2581.
- [13] M. Rungta, C. Zhang, W.J. Koros, L. Xu, Membrane-based ethylene/ethane separation: the upper bound and beyond, AIChE J. 59 (2013) 3475–3489.
- [14] N. Du, M.M. Dal-Cin, G.P. Robertson, M.D. Guiver, Decarboxylation-induced crosslinking of polymers of intrinsic microporosity (PIMs) for membrane gas separation, Macromolecules 45 (2012) 5134–5139.
- [15] A.M. Kratochvil, W.J. Koros, Decarboxylation-induced cross-linking of a polyimide for enhanced CO₂ plasticization resistance, Macromolecules 41 (2008) 7920–7927.
- [16] C. Zhang, P. Li, B. Cao, Decarboxylation crosslinking of polyimides with high CO₂/ CH₄ separation performance and plasticization resistance, J. Membr. Sci. 528 (2017) 206–216.
- [17] W. Qiu, C.-C. Chen, L. Xu, L. Cui, D.R. Paul, W.J. Koros, Sub-tg cross-linking of a polyimide membrane for enhanced CO₂ plasticization resistance for natural gas separation, Macromolecules 44 (2011) 6046–6056.
- [18] S.A. Stern, Y. Mii, H. Yamamoto, Structure/permeability relationships of polyimide membranes. Applications to the separation of gas mixtures, J. Polym. Sci. B Polym. Phys. 27 (1989) 1887–1909.
- [19] S.A. Stern, V. Saxena, Concentration-dependent transport of gases and vapors in glassy polymers, J. Membr. Sci. 7 (1980) 47–59.
- [20] L.M. Robeson, The upper bound revisited, J. Membr. Sci. 320 (2008) 390–400.
- [21] R.L. Scott, The anomalous behavior of fluorocarbon solutions, J. Phys. Chem. 62 (1958) 136–145.

- [22] E.M.D. Siebert, C.M. Knobler, Interaction virial coefficients in hydrocarbon-fluorocarbon mixtures, J. Phys. Chem. 75 (1971) 3863–3870.
- [23] N.L. Le, Y. Wang, T.-S. Chung, Synthesis, cross-linking modifications of 6FDA-NDA/ DABA polyimide membranes for ethanol dehydration via pervaporation, J. Membr. Sci. 415–416 (2012) 109–121.
- [24] C. Staudt-Bickel, W.J. Koros, Improvement of CO₂/CH₄ separation characteristics of polyimides by chemical crosslinking, J. Membr. Sci. 155 (1999) 145–154.
- [25] M.E. Dose, I. Hubacek, D.R. Paul, B.D. Freeman, CO₂, C₂H₄, and C₂H₆ sorption and mixed gas permeability of thermally cross-linked diaminophenylindane (DAPI) containing polyimides, J. Membr. Sci. (2018) In Preperation.
- [26] M.E. Dose, J.D. Moon, I. Hubacek, D.R. Paul, B.D. Freeman, Fundamental gas transport and dilation studies in thermally cross-linked diaminophenylindane (DAPI) containing polyimides, J. Polym. Sci. B Polym. Phys. (2018) In Preparation.
- [27] S.H. Han, N. Misdan, S. Kim, C.M. Doherty, A.J. Hill, Y.M. Lee, Thermally rearranged (TR) polybenzoxazole: effects of diverse imidization routes on physical properties and gas transport behaviors, Macromolecules 43 (2010) 7657–7667.
- [28] P.R. Bevington, D.K. Robinson, Error analysis, Data Reduction and Error Analysis, McGraw-Hill, New York, NY, 2003, pp. 36–50.
- [29] H. Lin, B.D. Freeman, Chapter 7: permeation and diffusion, Handbook of Materials Measurement Methods, Springer, 2006, pp. 371–387.
- [30] E.W. Lemmon, M.O. McLinden, D.G. Friend, Thermophysical properties of Fluid systems, in: P.J. Linstrom, W.G. Mallard (Eds.), NIST Chemistry WebBook, NIST Standard Reference Database Number 69, National Institute of Standards and Technology, Gaithersburg MD, 2018.
- [31] Z.P. Smith, D.F. Sanders, C.P. Ribeiro, R. Guo, B.D. Freeman, D.R. Paul, J.E. McGrath, S. Swinnea, Gas sorption and characterization of thermally rearranged polyimides based on 3,3'-dihydroxy-4,4'-diamino-biphenyl (HAB) and 2,2'bis-(3,4-dicarboxyphenyl) hexafluoropropane dianhydride (6FDA), J. Membr. Sci. 415–416 (2012) 558–567.
- [32] R.R. Tiwari, Z.P. Smith, H. Lin, B.D. Freeman, D.R. Paul, Gas permeation in thin films of "high free-volume" glassy perfluoropolymers: Part I, Physical Aging, Polymer 55 (2014) 5788–5800.
- [33] J.H. Kim, W.J. Koros, D.R. Paul, Physical aging of thin 6FDA-based polyimide membranes containing carboxyl acid groups. Part I. Transport properties, Polymer 47 (2006) 3094–3103.
- [34] P. Flory, J. Rehner, Statistical mechanics of cross-linked polymer chain networks II: swelling, J. Chem. Phys. 11 (1943) 521–526.
- [35] J.M. Salley, C.W. Frank, Charge transfer in aromatic polyimdes, in: M. Ghosh (Ed.), Polyimide: Fundamentals and Applications, Marcel Dekker, New York, 1996.
- [36] H. Kawakami, M. Mikawa, S. Nagaoka, Gas transport properties in thermally cured aromatic polyimide membranes, J. Membr. Sci. 118 (1996) 223–230.

- [37] J.M. Cervantes-Uc, J.V. Cauich-Rodríguez, H. Vázquez-Torres, A. Licea-Claveríe, TGA/FTIR study on thermal degradation of polymethacrylates containing carboxylic groups, Polym. Degrad. Stabil. 91 (2006) 3312–3321.
- [38] J.Y. Park, D.R. Paul, Correlation and prediction of gas permeability in glassy polymer membrane materials via a modified free volume based group contribution method, J. Membr. Sci. 125 (1997) 23–39.
- [39] M. Langsam, W. Burgoyne, Effects of diamine monomer structure on the gas permeability of polyimides. I. Bridged diamines, J. Polym. Sci. Polym. Chem. 31 (1993) 909–921.
- [40] D.R. Paul, Gas sorption and transport in glassy polymers, Reports of the Bunsen Society for Physical Chemistry 83 (1979) 294–302.
- [41] L.M. Robeson, M.E. Dose, B.D. Freeman, D.R. Paul, Analysis of the transport properties of thermally rearranged (TR) polymers and polymers of intrinsic microporosity (PIM) relative to upper bound performance, J. Membr. Sci. 525 (2017) 18–24.
- [42] L.M. Robeson, B.D. Freeman, D.R. Paul, B.W. Rowe, An empirical correlation of gas permeability and permselectivity in polymers and its theoretical basis, J. Membr. Sci. 341 (2009) 178–185.
- [43] M.S. McCaig, D.R. Paul, Effect of UV crosslinking and physical aging on the gas permeability of thin glassy polyarylate films, Polymer 40 (1999) 7209–7225.
- [44] C.T. Wright, D.R. Paul, Gas sorption and transport in UV-irradiated polyarylate copolymers based on tetramethyl bisphenol-A and dihydroxybenzophenone, J. Membr. Sci. 124 (1997) 161–174.
- [45] Y. Huang, D. Paul, Experimental methods for tracking physical aging of thin glassy polymer films by gas permeation, J. Membr. Sci. 244 (2004) 167–178.
- [46] D. Punsalan, W.J. Koros, Thickness-dependent sorption and effects of physical aging in a polyimide sample, J. Appl. Polym. Sci. 96 (2005) 1115–1121.
- [47] M. Rungta, L. Xu, W.J. Koros, Carbon molecular sieve dense film membranes derived from Matrimid® for ethylene/ethane separation, Carbon 50 (2012) 1488–1502.
- [48] A. Bos, I. Punt, H. Strathmann, M. Wessling, Suppression of gas separation membrane plasticization by homogeneous polymer blending, AIChE J. 47 (2001) 1088–1093.
- [49] L. Xu, M. Rungta, W.J. Koros, Matrimid® derived carbon molecular sieve hollow fiber membranes for ethylene/ethane separation, J. Membr. Sci. 380 (2011) 138–147
- [50] W. Qiu, L. Xu, C.-C. Chen, D.R. Paul, W.J. Koros, Gas separation performance of 6FDA-based polyimides with different chemical structures, Polymer 54 (2013) 6226–6235.
- [51] J.D. Wind, D.R. Paul, W.J. Koros, Natural gas permeation in polyimide membranes, J. Membr. Sci. 228 (2004) 227–236.